Science Advances
AAAS

advances.sciencemag.org/cgi/content/full/5/7/eaaw2326/DC1

Supplementary Materials for

Molecular basis of tRNA recognition by the Elongator complex

Maria I. Dauden, Marcin Jaciuk, Felix Weis, Ting-Yu Lin, Carolin Kleindienst, Nour El Hana Abbassi, Heena Khatter, Rościsław Krutyhołowa, Karin D. Breunig, Jan Kosinski*, Christoph W. Müller*, Sebastian Glatt*

*Corresponding author. Email: kosinski@embl.de (J.K.); cmueller@embl.de (C.W.M.); sebastian.glatt@uj.edu.pl (S.G.)

Published10 July 2019, *Sci. Adv.* **5**, eaaw2326 (2019)
DOI: 10.1126/sciadv.aaw2326

The PDF file includes:

Other Supplementary Material for this manuscript includes the following:

(available at advances.sciencemag.org/cgi/content/full/5/7/eaaw2326/DC1)

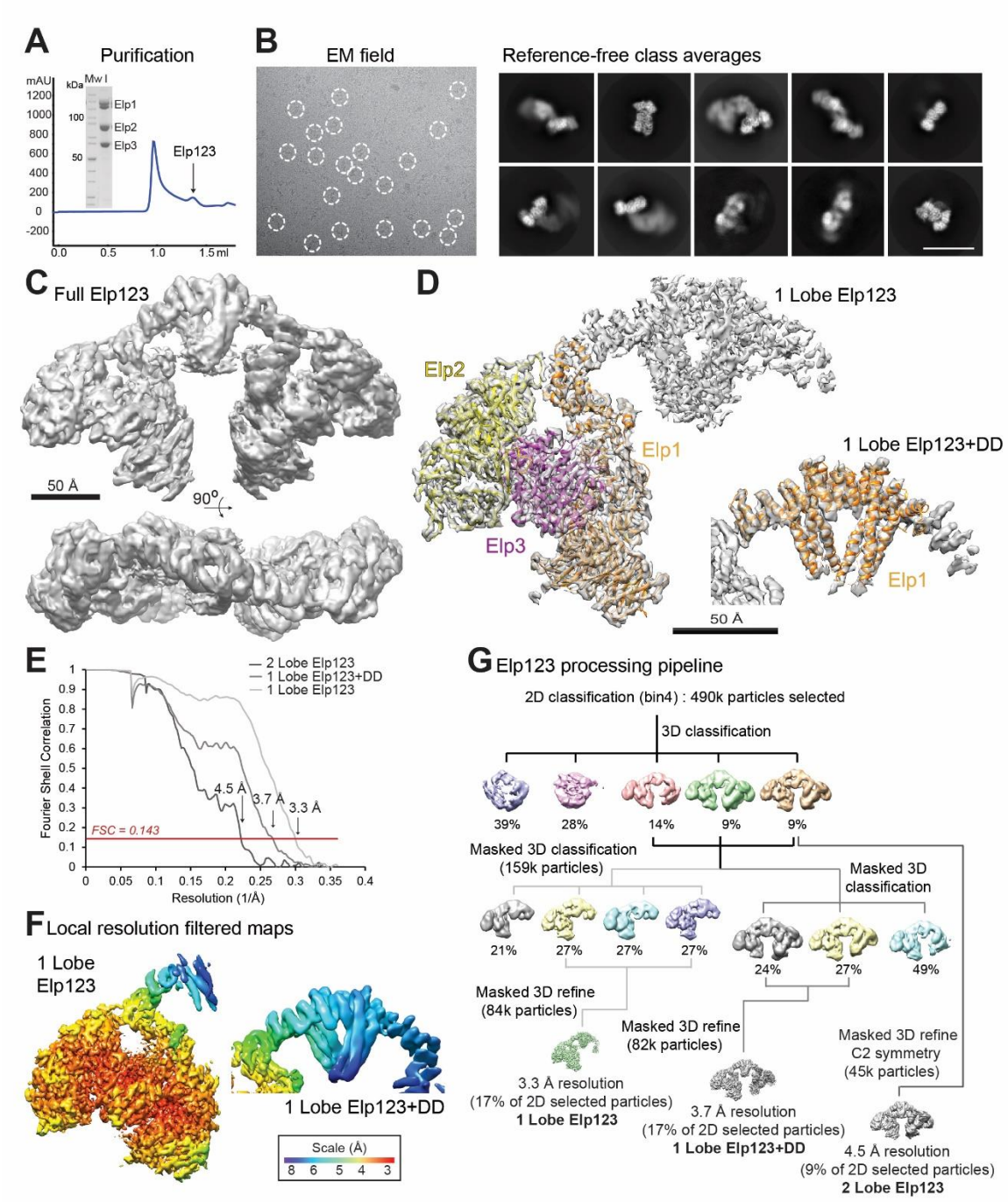

Fig. S1 Elp123 cryo-EM reconstruction. (**A**) SDS–PAGE gel showing the purified Elp123 complex and corresponding gel filtration profile. (**B**) Representative cryo-EM field of the Elp123 complex. Particles are highlighted. Reference-free class averages of the Elp123 dataset. Scale bar, 20 nm (right). (**C**) Two lobed reconstruction of the Elp123 at 4.5 Å resolution. (**D**) Locscale maps of the Elp123 lobe with and without the DD of Elp1 and the resulting atomic models. (**E**) Fourier Shell Correlation curve for different Elp123 reconstructions. The red line indicates FSC=0.143 and the individual resolution cutoffs are labeled. (**F**) The resolution range of the Elp123 lobe map is displayed on the local resolution filtered map. (**G**) General processing pipeline.

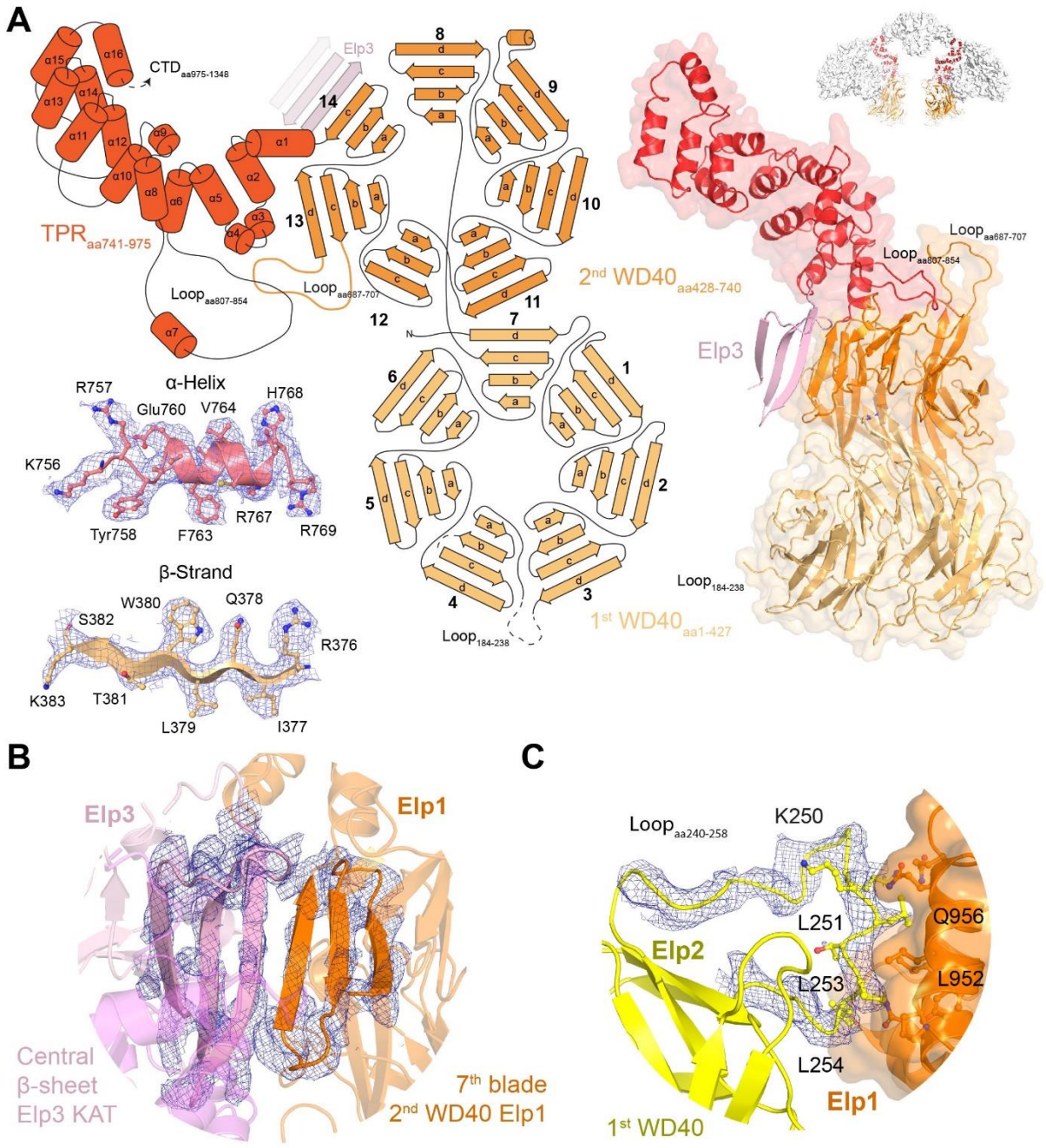

Fig. S2. Atomic structure of the Elp1 N terminus and intersubunit contacts. (**A**) Topological and atomic models of the N-terminal part of ScElp1. Representative densities of α-helices and β-strands are shown at a threshold level of 8. The structural models are depicted using cartoon and semi-transparent surface representation. (**B**) Close up of the interface between the KAT domain of Elp3 and the 2nd WD40 domain of Elp1, showing an antiparallel β-sheet complementation. (**C**) Close up of the interface between the 1st WD40 of Elp2 with the TPR region of Elp1. Respective loop density is shown and involved residues are labelled

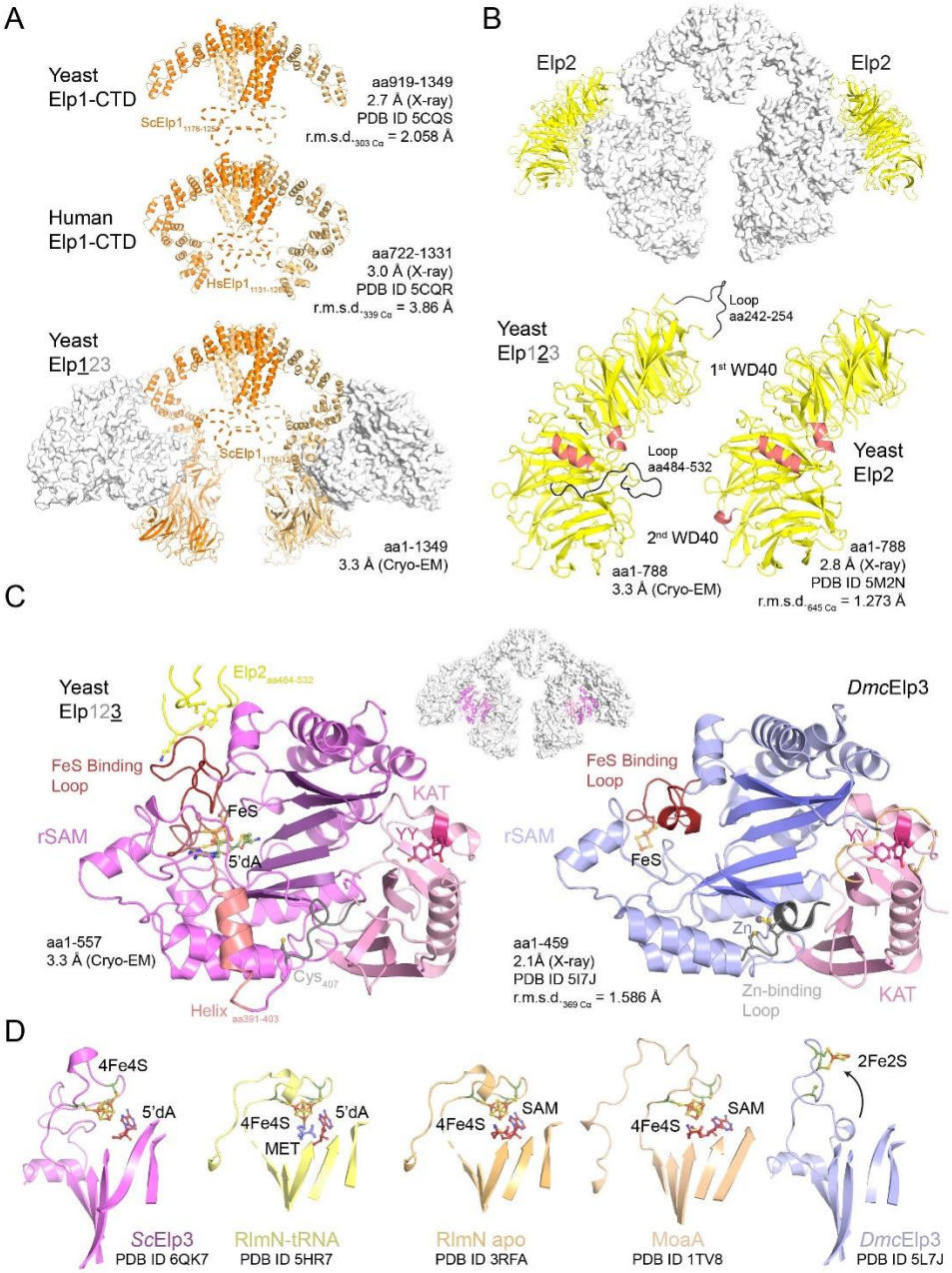

Fig. S3. Structural comparison of individual Elongator subunits. (**A**) Structural comparison between available crystal structures of the DD domain of yeast (PDB ID 5CQS) and human Elp1 (PDB ID 5CQR) with *Sc*Elp1 in the apo Elp123 complex. (**B**) Structural comparison between the available crystal structure of yeast Elp2 (PDB ID 5M2N) with ScElp2 in the apo Elp123 complex. (**C**) Structural comparison between the available crystal structure of *Dmc*Elp3 (PDB ID 5L7J) with *Sc*Elp3 in the apo Elp123 complex (PDB ID 6QK7). (**D**) Close up comparison between the position of the FeS cluster (orange/yellow) and SAM molecules (red) in *Sc*Elp3 with other rSAM proteins (RlmN PDB ID 5HR7/3RFA; MoaA PDB ID 1TV8) and *Dmc*Elp3. The structural models of the other subunits are depicted using white surface representation.

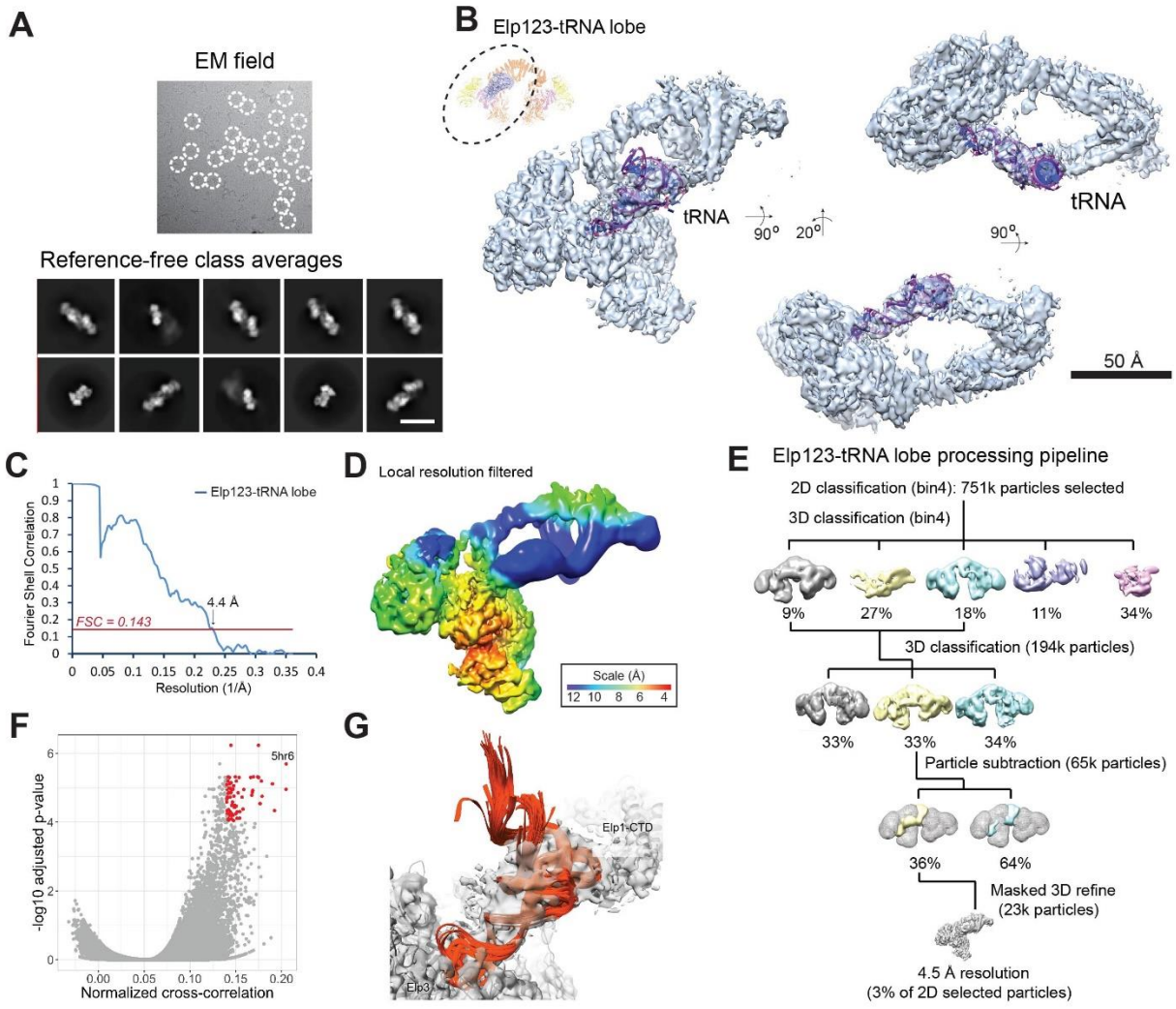

Fig. S4. Cryo-EM reconstruction of Elp123-tRNA. (**A**) Representative cryo-EM field of the Elp123-tRNA complex. Particles are highlighted. Reference-free class averages of the Elp123 dataset. Scale bar, 20 nm (right). (**B)** Different lobe reconstruction of the Elp123-tRNA complex from different perspectives showing representative densities and the fitted tRNA model. (**C**) Fourier Shell Correlation curve for the Elp123-tRNA reconstruction. The red line indicates FSC=0.143 and the resolution cutoff is labeled. (**D**) The resolution range of the Elp123-tRNA reconstruction is displayed on the local resolution filtered map. (**E**). General processing pipeline. (**F**) The volcano plot showing the fitting score (normalized "cross-correlation about the mean" calculated with UCSF Chimera, x-axis) versus the −log 10 adjusted p-values (y-axis) for around 4,000,000 alternative fits of the 802 tRNA structures retrieved from the Protein Data Bank. The top fits with the score higher than 0.15 and the −log 10 p-value higher than 4 (p-value lower than 10-4) are colored red. "5hr6" indicates the PDB ID of the tRNA template used for modeling of the tRNAAla. See Methods for how the fitting was performed and how the p-values have been calculated. (**G**) The top fits depicted in ribbon representation (orange red) within the EM map (grey envelope).

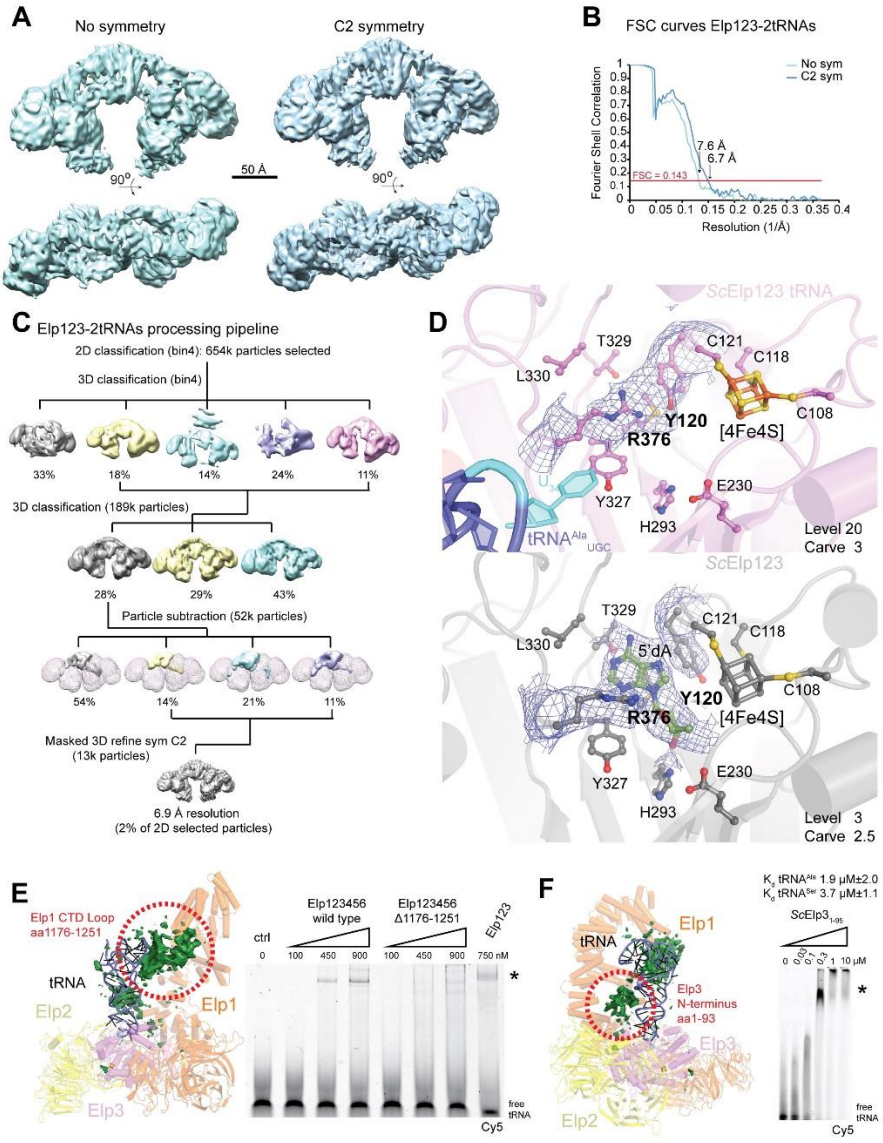

Fig. S5. Cryo-EM reconstruction of Elp123 bound to two tRNAs. (**A**) Different lobe reconstruction of the Elp123-2tRNA complex showing non-symmetrized (left) and symmetrized (right) densities from different perspectives. (**B**) Fourier Shell Correlation curve for non-symmetrized (light blue) and symmetrized (blue) Elp123-2tRNA reconstructions. The red line indicates FSC=0.143 and the resolution cutoff is labeled. (**C)** General processing pipeline. (**D**) Close up of the Elp3 active site in the tRNA-bound (top, colored) and unbound (bottom, grey) Elp123 structures. Cryo-EM densities for potentially rearranged residues (Y120 and R376; bold) and 5′dA (green) are shown at given threshold levels and carve values. Residue numbers, tRNA bases and FeS cluster are labeled (**E**) Model of Elp123-tRNA showing additional densities (green) that were not described by the model (left). EMSA assay using different concentrations of endogenous Elp123, recombinant Elongator complex and fluorescently labelled $tRNA^{Ala}_{UGC}$. Wild type and mutated Elongator were used and free tRNA and protein-tRNA complex (*) are indicated. (**F**) Same as D using purified N-terminus of Elp3 (aa1-95). Binding affinities from quantitative MST experiments are shown, n=3.

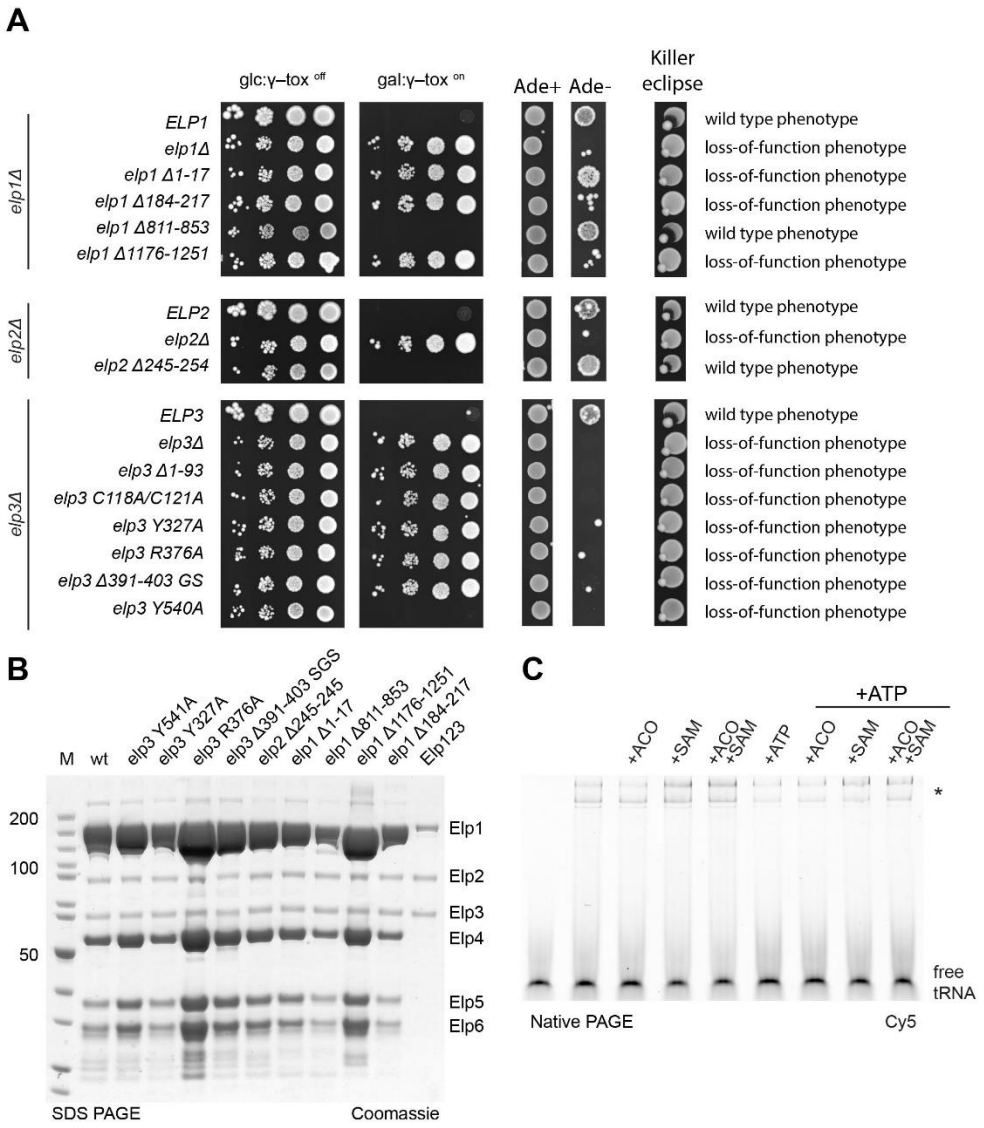

Fig. S6. In vivo and in vitro characterization of Elongator mutants. (**A**) Phenotypes of yeast strains carrying the indicated *elp1*, *elp2* and *elp3* mutant alleles using γ-toxin assay (transformation with galactose inducible GAL1-γ-toxin expression plasmid pLF16), *SUP4* suppression (growth on medium lacking adenine) and killer eclipse assays (*S. cerevisiae* strains inoculated with *K. lactis* killer strain AWJ137). Non-functional Elongator confers resistance against zymocin, but inhibits growth without adenine. γ-toxin, *SUP4* suppression and killer eclipse assays are described in detail in the Materials and Methods section. The zymocin resistance phenotype of *elp* mutants shown in Fig. 5C perfectly correlates with loss of *SUP4* mediated nonsense suppression creating an *Ade*- phenotype and the insensitivity to the zymocin secreted by a so-called killer strain AWJ137 of *Kluyveromyces lactis* confirming the loss of U_{34} tRNA modification. (**B**) SDS PAGE analysis of different purified Elongator variants. Amounts of proteins were normalized for Elp3 and visualized using Coomassie stain. (**C**) EMSA assay using recombinant Elongator and fluorescently labelled $tRNA^{Ala}_{UGC}$ in the presence of different combinations of acetyl-CoA (ACO), SAM and ATP. The positions of free tRNA and protein-tRNA complexes (*) are indicated next to the native PAGE.

Table S1. Collection and refinement statistics.

	***Sc*Elp123 (EMD-4571) (PDB 6QK7)**	***Sc*Elp123-tRNA (EMD-4574)**	***Sc*Elp123-2tRNAs (EMD-4576)**
Data collection and processing			
Magnification	105,000 x	105,000 x	105,000 x
Voltage	300 kV	300 kV	300 kV
Electron exposure ($e^-/Å^2$)	43	44	39.8
Defocus range (μm)	1-2.5	1-2.5	1-2.5
Pixel size (Å)	1.35	1.35	1.35
Symmetry imposed	Yes	no	yes
Initial images (no.)	4614	6990	5412
Final particle (no.)	84,135	23,020	12,921
Map resolution (Å)	3.3	4.4	6.7
FSC threshold	0.143	0.143	0.143
Map resolution range (Å)	3-5	4-12	-
Refinement			
Map sharpening B factor ($Å^2$)	-20	-40	-70
Model Composition			
Non-hydrogen atoms	20,790		
Protein residues	2,594		
Ligand	26		
R. m. s deviations			
Bond lengths (Å)	0.0050		
Bond angles (°)	1.07		
Validation			
MolProbity score	1.87		
Clashscore	6.27		
Poor rotamers (%)	0.49		
Ramachandran plot			
Favored (%)	90.68		
Allowed (%)	9.32		
Disallowed (%)	0.00		

Table S2. Yeast strains used in this study.

Strain	Relevant genotype	Source
AWJ137	*MATa, leu2, trp1, [k1+k2+]*	Kamper et al. (64)
UMY2893	*MATα SUP4 leu2-3,112 trp1-1 can1-100 ura3-1 ade2-1 his3-11,15*	Huang et al. (23)
SCCM49	*MATa; his3Δ1; leu2Δ0; met15Δ0, ura3Δ0; YLR384C-3xFLAG::natNT2*	this study
CKY27	UMY2893, *elp1Δ::KlURA3*	this study
CKY28	UMY2893, *elp2Δ::KlURA3*	this study
CKY29	UMY2893, *elp3*_Δ391-403+SGS-linker	this study
CKY30	UMY2893, *elp3*_R376A	this study
CKY31	UMY2893, *elp2*_Δ245-254	this study
CKY32	UMY2893, *elp3*_Y327A	this study
CKY34	UMY2893, *elp1*_Δ184-217	this study
CKY36	UMY2893, *elp1*_Δ1176-1251	this study
CKY37	UMY2893, *elp1*_Δ811-853	this study
CKY38	UMY2893, *elp3*_Δ1-93	this study
CKY39	UMY2893, *elp1*_Δ1-17	this study
ONY14	UMY2893, *elp3Δ::KlURA3*	Glatt et al. (29)
RZY91	UMY2893, *elp3*_Y540-*(myc)$_3$::SpHIS5*	R. Zabel
RZY106	UMY2893, *elp3*_C118A/C121A-*(myc)$_3$::SpHIS5*	R. Zabel